PHYSICAL REVIEW B VOLUME 9, NUMBER 10 15 MAY 1974

Far-infrared recombination radiation from n-type Ge and GaAs[†]

Stephen R. Thomas* and H. Y. Fan
Department of Physics, Purdue University, Lafayette, Indiana 47907
(Received 15 November 1973)

Far-infrared radiation given by the impact ionization of Ge and GaAs at ~4 °K has been studied. The semiconductors studied include Ge(Sb), Ge(As), Ge(P), and epitaxial n-GaAs with an unidentified shallow impurity. The impact ionization is produced by electrical pulses applied to the specimen and studies are made with pulses of various amplitudes. The spectrum of the emitted radiation in the range 70–400 μm is measured using a Michelson interferometer. Sharp peaks in the spectra are attributable to electron transitions between various impurity states which can be identified, and the electron occupation under impact ionization is determined for some of the impurity states. Transitions of conduction electrons to the impurity states give a broad band in the observed spectra. Considerations show that a hydrogenic approximation may be used for the cross section for radiative recombination, with which the energy distribution of conduction electrons is determined form studies of the broad band.

I. INTRODUCTION

Impact ionization in semiconductors is now a well-known effect. In the case of shallow impurities which bind carriers at low temperature, impact ionization can be produced by moderate electric fields. Recombination of the ionized carriers with the impurity may occur radiatively giving emission in the far infrared which is an interesting spectral range. Such emission was first reported by Koenig and Brown[1] for germanium containing Sb or As impurity; the emission was detected by the photoconductive response of another piece of germanium with Sb or As impurity. Ascarelli and Brown[2] observed an increase of the noise detected as a dc breakdown field was applied to a Ge(Sb) sample and attributed the effect to recombination radiation from the sample. Salomon and Fan[3] observed recombination radiation from Ge(Sb) and p-InSb and obtained emission spectra in the form of histograms by using various combinations of filters. A Michelson interferometer was used by Melngailis *et al.*[4] to obtain some emission spectra from epitaxial GaAs. Emission spectra were studied by Gornik[5] for n-InSb in a magnetic field; features of the spectra were interpreted as electron transitions between impurity states, transitions between the first Landau level and the ground state of the impurity, and transitions between the first two Landau levels. Some evidence for emissions associated with transitions from the second Landau level to an impurity state and to the lowest Landau level in n-InSb was also reported recently by Kobayashi *et al.*[6] It appears that more detailed studies will be helpful for the understanding of various significant factors involved.

Investigations of recombination emission from germanium containing different donor impurities and from epitaxial n-type GaAs are reported in this paper. Emission spectra were measured with a far-infrared interferometer. Measurements were made at various pulsed electric fields which produced the impact ionization. The sharp peaks in the spectra are attributed to electron transitions among impurity states which are identified. The electron occupation is determined for some of the states. The observed broad band in each spectrum corresponds to transitions of the conduction electrons to the localized states of the ionized impurity. The radiative capture cross section is deduced by considering the fit of available absorption data with existing theories. Using the capture cross section, the energy distribution of the conduction electrons is determined from analysis of the broad band. The prospect for obtaining stimulated emission is considered using results of the measurements.

II. EXPERIMENTAL ARRANGEMENT

The schematic diagram of the experimental setup is given in Fig. 1. A Michelson interferometer, Grubb Parsons model MK II, was used. The sample to be measured and the emission detector were placed in separate Dewars which were situated in a common housing with the interferometer. The housing could be evacuated to remove sufficiently water vapor which would cause absorption. A TPX lens in front of the sample Dewar served to collimate the emitted radiation. The radiation was focused on the detector by a lens in front of the detector Dewar, a polyethylene lens in case of the Ge(Sb) detector or a TPX lens in case of the GaAs detector.

The Ge samples were etched in CP_4 and contacts were put on with 35-at.%-Sn–63-at.%-Pb–2-at.%-Sb solder and stainless-steel flux. Contacts on the epitaxial GaAs sample were made using 66-at.%-Sn–32-at.%-In–2-at.%-Sb solder dissolved in mercury and alloying in a nitrogen atmosphere at 425 °C for 30 min. Electrical pulses producing impact ionization in the sample were provided by

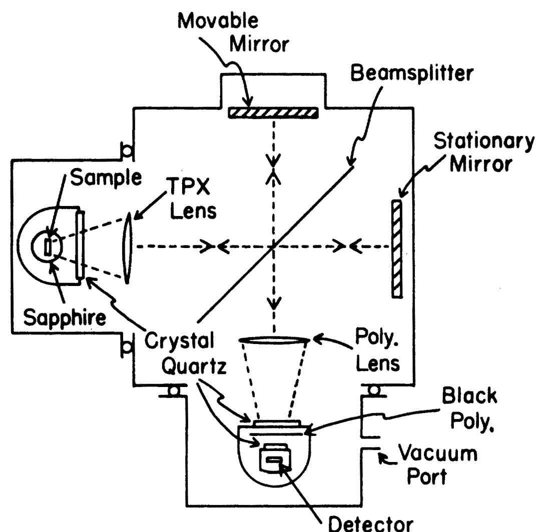

FIG. 1. Schematic diagram of the optical system.

a Hewlett Packard 214A pulse generator which was capable of delivering a maximum current of 2 A into a 50-Ω load. The movable mirror of the interferometer was driven by a motor in discrete steps, giving an optical path difference of 5 μm per step, and the stepping time could be chosen to be appropriate for the time constant of the detection system. The signal output of the detector was fed into a boxcar integrator or a lock-in amplifier which was triggered by the pulse generator. The signal given by the boxcar integrator or the lock-in amplifier was fed into a recorder and was digitized by an encoder. The binary-coded output of the encoder was fed into a control chassis which was triggered in synchronism with the stepping of the movable mirror of interferometer. The encoder output at the instant of each triggering was stored and delivered as sequential digital output to an IBM card punch, giving an interferogram. The Fourier transform of the interferogram obtained by means of a computer yielded the spectrum of the detected radiation.

The sample measured was immersed in liquid helium contained in the sapphire tail piece of a glass cryostat. The cryostat window was crystalline quartz. The Ge(Sb) detector used was fixed to the cold finger of a liquid-helium cryostat and was electrically insulated from the cold finger except at the point of contact by 0.00025-in. Mylar. The detector was enclosed in a brass shield with a window of crystalline quartz. A filter of black polyethylene was also provided which was kept at liquid-nitrogen temperature. The window of the cryostat was made of crystalline quartz. The GaAs detector used was supplied by Molectron Corporation. The metal Dewar of this detector had windows of crystalline quartz. The detector was in a metal cavity with a window of crystalline quartz and black polyethylene, all of which were at liquid-helium temperature. The load resistor and the preamplifier of the detector were also contained in the Dewar. They were kept cold in order to reduce the noise and achieve faster response times.

Most of the measurements were made with two extrinsic photoconductive detectors, Ge(Sb) and GaAs. The detectors were calibrated against a Golay detector of known responsivity using the interferometer and a Hg lamp as the source. By comparing the measured spectra, we obtained the relative spectral responsivity shown in Figs. 2 and 3 for the two detectors. Since the interferometer gives a spectrum rather than a monochromatic radiation, the absolute values of the curves were determined in the following way. The noise equivalent power $\mathfrak{N}$ of the detector for radiation of wave number k is

$$\mathfrak{N}_k = v/R_k(\Delta f)^{1/2} \quad , \tag{1}$$

where v is the rms noise voltage, and Δf is the bandwidth of the amplifying system. The responsivity R_k is the ratio of rms signal voltage to rms incident radiation power P_k. The expression may

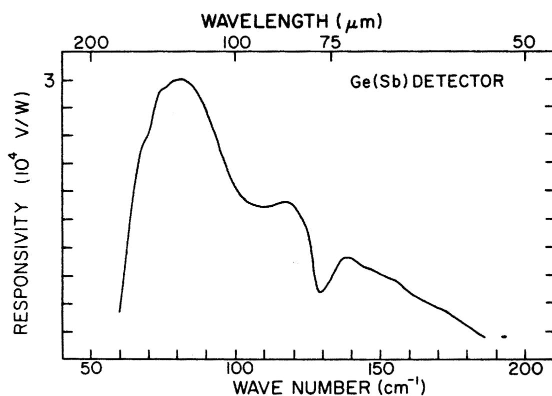

FIG. 2. Spectral response of Ge(Sb) detector. Resolution about 3 cm^{-1}.

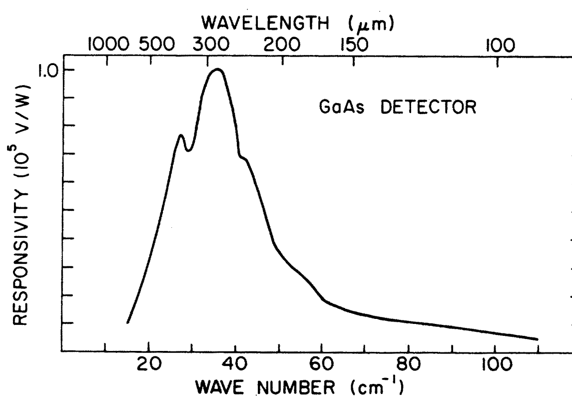

FIG. 3. Spectral response of GaAs detector. Resolution about 2 cm^{-1}.

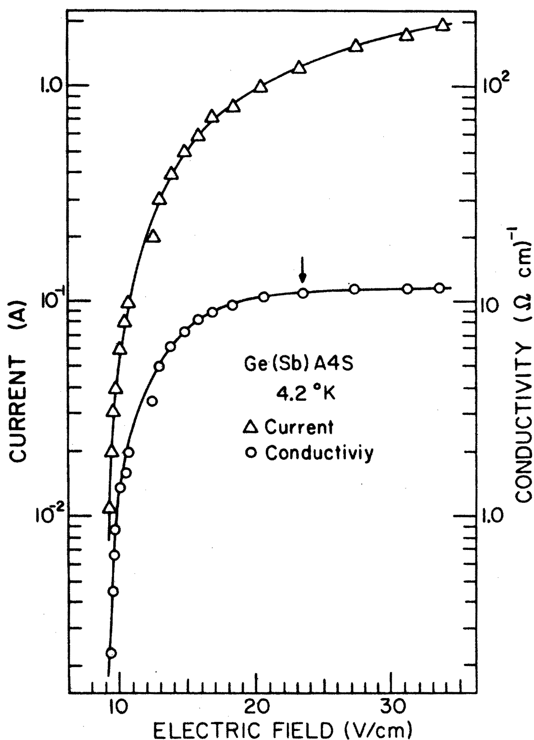

FIG. 4. Current and conductivity vs electric field for Ge(Sb)-$A4S$. The data were taken for a 20-μsec pulse width at 20 Hz.

be rewritten

$$\mathfrak{N}_k=\frac{v}{(\Delta f)^{1/2}}\,\frac{P}{\sum_{k'}P_{k'}R_{k'}}\sum_{k'}\frac{P_{k'}}{P}\,\frac{R_{k'}}{R_k}\ ,\qquad (2)$$

where $P=\sum_{k'}P_{k'}$ is the total incident power over the spectral range. The sum $\sum_{k'}P_{k'}R_{k'}$ is the rms signal voltage produced by P, which can be obtained from the central maximum of the interferogram. P and the spectrum of P_k/P are given by the spectrum obtained with the Golay detector. $R_{k'}/R_k$ is given by the spectral responsivity. Therefore we can calculate the value of $\mathfrak{N}_k$ using (2) and then calculate the value of R_k using (1). The values of $\mathfrak{N}_k$ at the peak of the responsivity were 7×10^{-11} and 2×10^{-12} W/Hz$^{1/2}$ for the Ge(Sb) and GaAs detectors, respectively. The Ge(Sb) detector was used for studies of spectra above ~ 60 cm^{-1}, and the GaAs detector was used in studying the range of lower wave numbers.

Only a fraction of the emitted radiation was detected. The attenuation factor is determined by the optical geometry and transmissions of the filters, windows, and interferometer. Regarding the optical geometry, the sample was considered to be radiating according to Lambert's cosine law. The estimated over-all attenuation factors were in the range of 5×10^{-4} to 2×10^{-3} for the various measurements. When the interferometer did not have to be used, the sample Dewar and the detector Dewar were connected directly by a light pipe. By eliminating the attenuation due to the interferometer and lenses, weaker emissions could be studied.

III. SIGNAL OF TOTAL EMISSION

Single-crystal samples of germanium doped with various impurities and samples of epitaxial n-GaAs with unknown impurity were studied. Table I lists the samples on which most of the measurements were made. Figures 4–7 show the conductivity and current as functions of the electric field for the samples. The measurements were made with four probes, two potential probes in addition to the current contacts. The results obtained were independent of current direction. Careful checks made previously[3] in this laboratory showed no significant indication of carrier injection or extraction from the current contacts, for Ge samples giving similar results. With the exception of the curves for Ge(As)-$C2S$, the curves have the familiar shape. A steep rise at some field due to the sharp increase of impact-ionized carriers leads to a plateau where the conductivity may increase or decrease slightly with increasing field. The number of free carriers approaches a saturation, and the small variation of conductivity comes

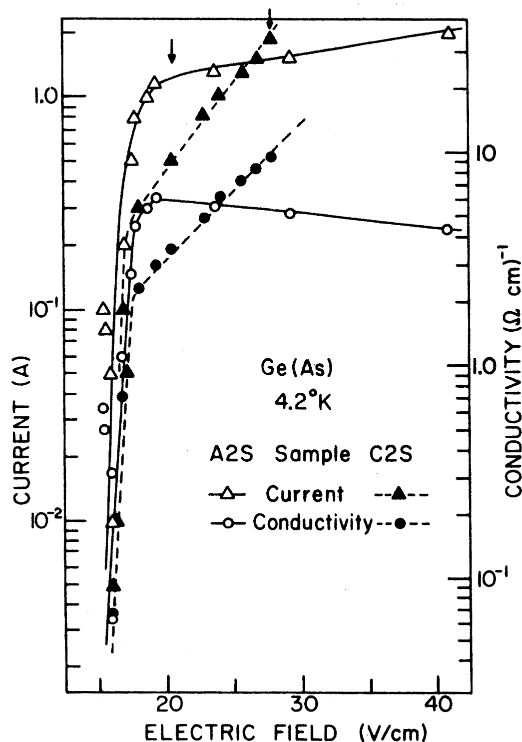

FIG. 5. Current and conductivity vs electric field for the Ge(As) samples. The data were taken for a 30-μsec pulse width at 110 Hz.

TABLE I. List of samples.

Sample	Carrier concentration at 300 °K (cm^{-3})	Sample dimension (mm)	Supplier
Ge(Sb)-*A4S*	1.6×10^{15}	$6.4\times1.73\times0.27$	Purdue
Ge(As)-*A2S*	9.1×10^{14}	$6.8\times1.9\times0.53$	Purdue
Ge(As)-*C2S*	3.5×10^{14}	$7.3\times2.5\times0.27$	Purdue
Ge(P)-*A1S*	4.4×10^{14}	$7.3\times2.4\times0.50$	Purdue
n-GaAs-*B5S*, epitaxial	3.34×10^{15}	$7.2\times3.6\times0.115$	Monsanto

largely from a variation of average carrier mobility, which depends on the carrier distribution in the energy band. The conductivity of Ge(As)-*C2S* shows a stronger variation after bending from the steep rise than the other samples in their plateau regions. The reason for the somewhat unusual behavior is not clear.

The radiation emitted was measured by using the Ge(Sb) detector with a light-pipe connection between the Dewars for the sample and the detector. The strength of emission signal is plotted in Fig. 8 for the Ge(Sb) sample. Two sets of data are shown which were obtained with the liquid He surrounding the sample pumped or not pumped. The pulses of emission as shown by an oscilloscope had a rise time of ~15 μsec, consistant with the characteristic of the detector-circuit response. Electrical pulses of a width of 20 or 30 μsec and a repetition rate of < 110 Hz were used in this work. The emission pulse dropped to a negligible level at the end of an electrical pulse, in agreement with the previous report of Salomon and Fan.[3] The long tail, called afterglow, which had been observed and attributed to sample heating at long pulse widths, became noticeable only at pulse widths of ≳60 μsec. Assuming the sample cooled between pulses and heated adiabatically during each pulse, the temperature reached during a pulse is estimated to be ~20 °K. The assumption of adiabatic heating makes the estimate an upper limit. The temperature reached must have been considerably lower when the liquid He was pumped.

The signal is seen to be proportional to the sam-

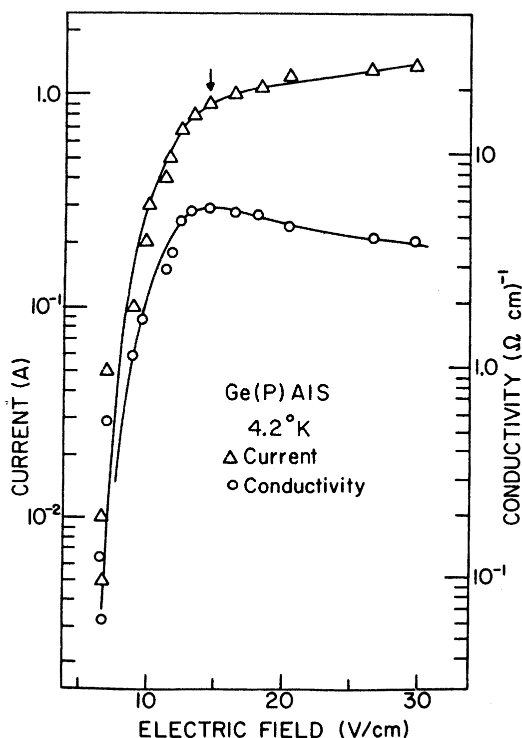

FIG. 6. Current and conductivity vs electric field for Ge(P)*A1S*. The data were taken for a 30-μsec pulse width at 110 Hz.

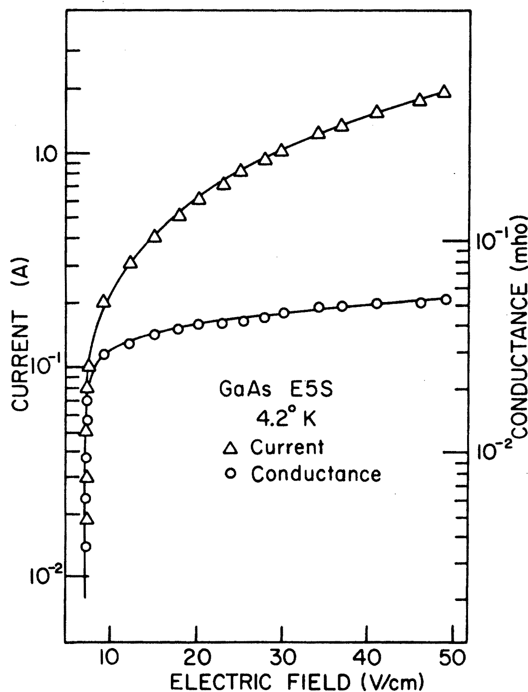

FIG. 7. Current and conductivity vs electric field for GaAs-*E5S*. The data were taken for a 30-μsec pulse width at 100 Hz.

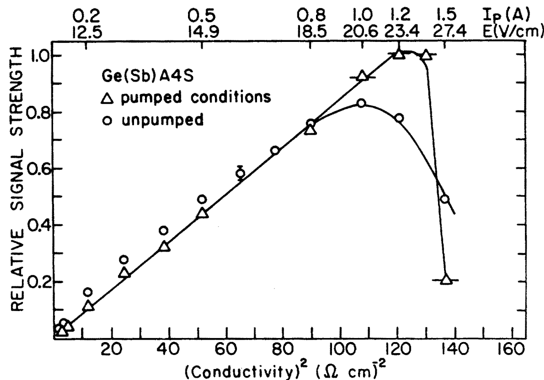

FIG. 8. Detected emission signal vs conductivity squared for Ge(Sb)$A4S$. Data are given both for normal and for pumped liquid-helium conditions. The temperature of pumped He was below 2.17 °K.

ple conductivity squared σ^2 up to an electric field $E \sim 23$ V/cm. All the Ge samples studied showed such behavior, which is consistent with the observations of Salomon and Fan on Ge(Sb). The electric field up to which the σ^2 relation holds is indicated by an arrow in Figs. 4–6. It is seen that the relation was found to hold from the steeply rising part to some point after the bending of the $\sigma(E)$ curve. The relation can be explained by the following consideration. The recombination emission may be expected to be proportional to the product of the concentration n of carriers and the concentration N^+ of relevant impurity atoms. In case of small doping compensation, $N^+ \simeq n = \sigma/e\langle\mu\rangle$ and the emission intensity $\mathcal{E} = Bn^2$, where B is an average radiative recombination coefficient and $\langle\mu\rangle$ is the average mobility of the carriers. We get $\mathcal{E} \propto \sigma^2$ if $B/\langle\mu\rangle^2$ does not have an important variation.

The simple and common correlation of emission and conductivity did not hold at higher fields. The conductivity of Ge(Sb)-$A4S$ kept increasing slightly for fields beyond that indicated by the arrow in Fig. 4 but the emission signal dropped from the maximum. The conductivity of Ge(As)-$A2S$ and that of Ge(P)-$A1S$ dropped somewhat, while the emission signal of the first stayed constant and that of the second began to decrease. Finally, the conductivity of Ge(As)-$C2S$ continued to increase up to the highest field applied, where the emission signal just began to decrease from its maximum. The maximum emission power in the range 60–140 cm^{-1}, per unit volume of the sample, was 6×10^{-4}, 4×10^{-4}, 2×10^{-4}, 1.2×10^{-4} W/cm^3 for the samples Ge(Sb)-$A4S$, Ge(As)-$C2S$, Ge(As)-$A2S$, Ge(P)-$A1S$, respectively. Of the two As-doped samples, the sample with a higher impurity concentration did give a higher emission per unit volume. The explanation given in the preceding paragraph for the $\mathcal{E} \propto \sigma^2$ relation is a rough consideration. B and $\langle\mu\rangle^2$ may vary where the field is varied over a wide range, especially when the impact ionization is near saturation within the range covered. Furthermore, the intensity distribution may vary in the emission spectrum with variation of the field, which affects the signal given by a detector with nonuniform spectral responsivity. In addition, the two sets of data shown in Fig. 8 indicate that the emission signal at high fields was affected by the change of sample temperature. To attempt to explain the relation between the conductivity and the emission signal at high fields does not appear rewarding.

The emission signal of the epitaxial GaAs sample is shown in Fig. 9. The emission signal measured with a pulse width of 30 μsec continued to increase at the highest currents used. Similar behavior had been reported[4] for epitaxial GaAs in measurements using a 20-μsec pulse width, while emission measured with a 200-μsec pulse width was reported to decrease at high currents owing to heating effects. In contrast to the signal of the Ge samples, the signal seems to be proportional to conductance instead of conductance squared over the entire range of applied field. The linear relationship was observed also by Melngailis *et al.*[4] on epitaxial GaAs in the breakdown region of steadily rising conductance. The explanation given invoked the model of filamentary breakdown.[7] According to this model, the carriers are concentrated into filaments rather than distributed uniformly in the sample. The current increases as the filaments increase in volume at constant current densities. Consequently, the fraction of carriers recombining radiatively remains constant and the emission $\mathcal{E}$ is proportional to the number of carriers instead of the number squared for the case of uniform carrier distribution. If the average carrier mobility were nearly constant, the emission in the case of fila-

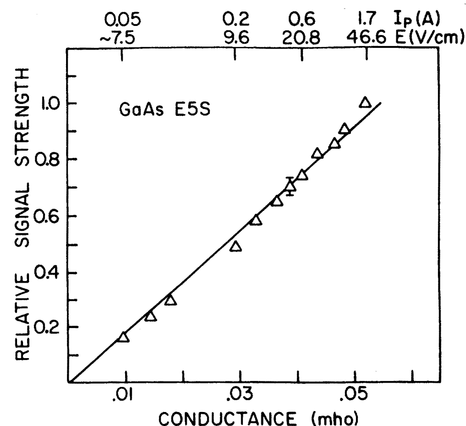

FIG. 9. Detected signal strength vs conductance for GaAs-$E5S$.

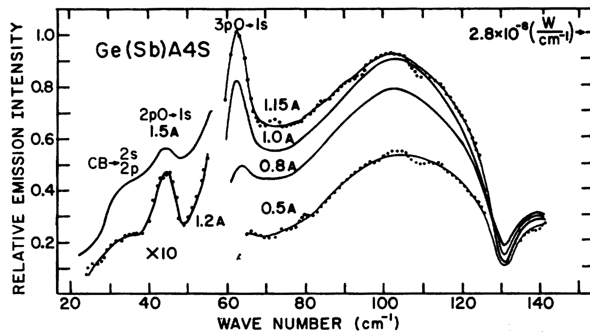

FIG. 10. Ge(Sb)-*A4S* emission spectra.

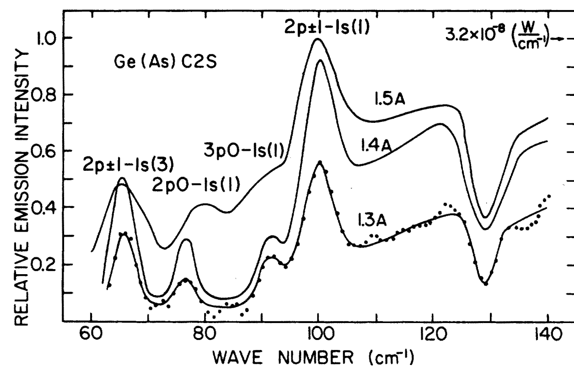

FIG. 12. Ge(As)-*C2S* emission spectra.

mentary breakdown would be proportional to the conductance rather than the conductance squared. However, the emission data in Fig. 9 covers the entire, nearly flat part of the conductivity curve in Fig. 8, where the constancy of carrier mobility is very questionable. Therefore, our emission data cannot be explained simply by filamentary breakdown.

IV. EMISSION SPECTRA OF GERMANIUM

A. Spectra

The emission spectra of the germanium samples are shown in Figs. 10–13. The spectra region above 60 cm^{-1} was measured with the Ge(Sb) detector and the GaAs detector was used for the region below 60 cm^{-1} in Figs. 10 and 13. Spectra measured with various pulsing currents are shown. The dip in the spectra near 130 cm^{-1} shows the effect of a crystalline quartz filter used in the optical path. The effect was taken into account in our considerations. Each of the spectra consists of some sharp peaks and a broad band at photon frequencies higher than the ionization energy of the impurity. Apparently, the band is given by transitions of conduction electrons to the impurity states while each sharp peak is associated with electron transitions between two localized impurity states.

The frequency of a sharp peak corresponds to the energy separation of two impurity states. The energy levels of the three impurities are listed in Table II according to the available absorption spectra[8] and calculated values[9] of 2*s*, 3*s*, and 4*s*. By using this table, transitions associated with the peaks are identified as indicated in Figs. 10–13. The following remarks may be made: (i) In the case of Sb impurity, the energy difference between 1*s*(1) and 1*s*(3) states is too small for transitions to these two states to be resolved with an experimental resolution of ~ 5 cm^{-1} for the emission. (ii) For all the impurities, the observed peaks are associated with transitions to the 1*s* states only. Transitions to higher states are not expected to give sharp peaks in the spectral region explored; transitions to the next higher state, 2*p*, 0 may give resolvable peaks only at wave numbers considerably smaller than the energy from 2*p*, 0 to the continuum *I*, i.e., considerably smaller than ~ 34 cm^{-1} for all the impurities. In the case of Sb impurity, transitions 4*s* → 2*p*, 0 correspond to ~ 28 cm^{-1}. The fact that the spectrum is generally weak at this end indicates the ineffectiveness of such transitions. (iii) On the side of large wave numbers, no peaks due to transitions from 3*p*, ± 1 or higher states are resolved since these states are close together,

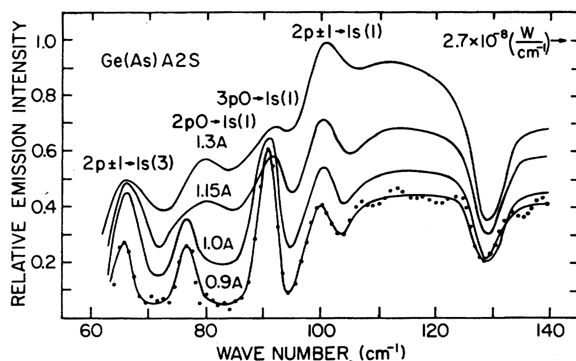

FIG. 11. Ge(As)-*A2S* emission spectra.

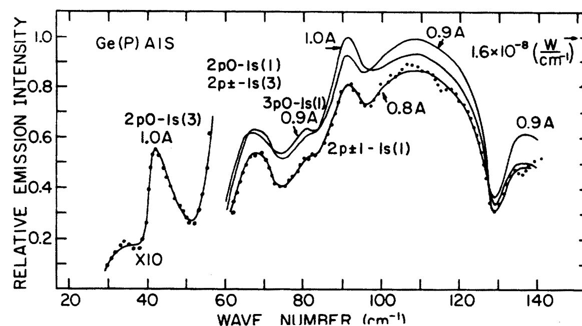

FIG. 13. Ge(P)-*A1S* emission spectra.

TABLE II. Energies of impurity states referred to the energy of the ground state $1s(1)$, according to Refs. 8 and 9. The values are given in units of meV and cm^{-1}. The values in cm^{-1} are given in parentheses. CB denotes the lowest state of conduction band. I denotes the lowest edge of unresolved absorption data.

	States above 1s (1)									
Impurity	1s (3)	2p, 0	2s	3p, 0	3s	2p, ±1	4s	3p, ±1	I	CB
Sb	0.32 (2.58)	5.58 (44.96)	6.67 (53.75)	7.75 (62.45)	8.18 (65.91)	8.59 (69.25)	9.02 (72.68)	9.29 (74.86)	9.66 (77.84)	10.19 (82.11)
As	4.23 (34.08)	9.44 (76.06)	10.52 (84.77)	11.61 (93.55)	12.03 (96.93)	12.44 (100.27)	12.87 (103.70)	13.15 (105.96)	13.65 (110)	14.04 (113.13)
P	2.83 (22.70)	8.15 (65.67)	9.24 (74.46)	10.33 (83.24)	10.75 (86.62)	11.16 (89.96)	11.59 (93.39)	11.84 (95.41)	12.36 (99.60)	12.76 (102.82)

separated by $\lesssim 4$ cm^{-1} from a "continuum" of states I. (iv) The fact that $2p, \pm 1 \to 1s$ peaks are evident in the spectra of Ge(As) and Ge(P) but are not noticeable in the spectra of Ge(Sb) seems to be an effect of the nature of the impurity. (v) The transitions $2s \to 1s$ and $3s \to 1s$ would give peaks in the wave-number range being observed. No peaks in any of the spectra can be identified with such transitions. The transition probability is expected to be very low for such transitions even when the surrounding of an impurity atom is considered realistically to have a T_d symmetry rather than a spherical symmetry. Apparently, these states are not so overwhelmingly populated as to give resolvable peaks in emission.

B. Population of impurity states

The calculation of N_j impurity atoms in an excited state j may be determined from the rate $\mathcal{E}_{jm}$ of photon emission per unit volume, which is given by electron transitions from the state j to a lower state m:

$$N_j = \mathcal{E}_{jm} / [8\pi\eta^2 (\nu/c)^2 (g_m/g_j) \sigma_{mj}] \quad , \tag{3}$$

where the denominator in square brackets is the Einstein coefficient for spontaneous $j \to m$ transition, η is the refractive index of the material, ν is the transition frequency, c is the speed of light in vacuum, g_j and g_m are, respectively, the degeneracies of states j and m, and σ_{mj} is the integrated absorption cross section for the $m \to j$ transitions which can be obtained from impurity absorption data. Consider the spectrum of Ge(Sb)-$A4S$ for $I_p \sim 1.2$ A and the spectrum for Ge(As)-$A2S$ for $I_p = 0.9$ A, the sharp bands of which can be resolved with least uncertainty. Using the values of σ_{mj} estimated from the available absorption data, we obtain the information given in Table III. Regarding the $2p, \pm 1$ and $3p \pm 1$ states in Ge(Sb)-$A4S$, no peaks corresponding to transitions from these states to $1s$ are noticeable in the emission spectrum, in contrast to the $3p, 0 \to 1s$ transition. Yet the transition probabilities for these states are several times higher than that of $3p, 0 \to 1s$ according to the absorption data. The population of each of the two states is thus estimated to be at least an order of magnitude lower than the population of $3p, 0$. Similar considerations apply to $3p, \pm 1$ in Ge(As)-$A2S$.

The population of each of the various states is determined by the balance between the transition rates to and from the state to all other states through all possible transition processes. The following simple consideration appears to be important for understanding the fact that $N_{2p,\pm1}$ and $N_{3p,\pm1}$ are much smaller than $N_{3p,0}$. The capture of a conduction electron through the most important process of phonon interaction is much more probable for s states,[10] i.e., states with $l = 0$ and $m = 0$. Furthermore, transitions through phonon interaction cannot occur from a state with $m = 0$ to a state with $m \neq 0$.[11] Consequently, the population of a $m \neq 0$ state tends to be lower than that of a $m = 0$ state. More detailed considerations are necessary to understand the difference between $N_{2p,0}$ and $N_{3p,0}$, both of which states have $m = 0$.

An inspection of the spectra for Ge(As) samples shows the population of $3p, 0$ did not increase as fast as that of $2p, \pm 1$ in the range of current used. The spectra for Ge(Sb)-$A4S$ shows that the $3p, 0 \to 1s$ emission in this sample increased faster than the broad band, indicating perhaps a faster growth of the population of $3p, 0$ than that of the conduction band. On the other hand, this behavior is not clearly seen in the spectra of the Ge(As) samples for the range of I_p investigated. We must bear in mind that the emission involving conduction electrons depends on the energy distribution of the

TABLE III. Concentration of impurity atoms in various states. N_D is the concentration of impurity atoms.

	I_p (A)	E (V/cm)	$N_{3p,0}/N_D$	$N_{2p,0}/N_{3p,0}$	$N_{2p\pm1}/N_{3p,0}$	$N_{3p,\pm1}/N_{3p,0}$
Ge(Sb)-$A4S$	1.15	23	~0.1	~0.1	<0.1	<0.1
Ge(As)-$A2S$	0.9	18	~0.08	~1/4	~1/20	<0.1

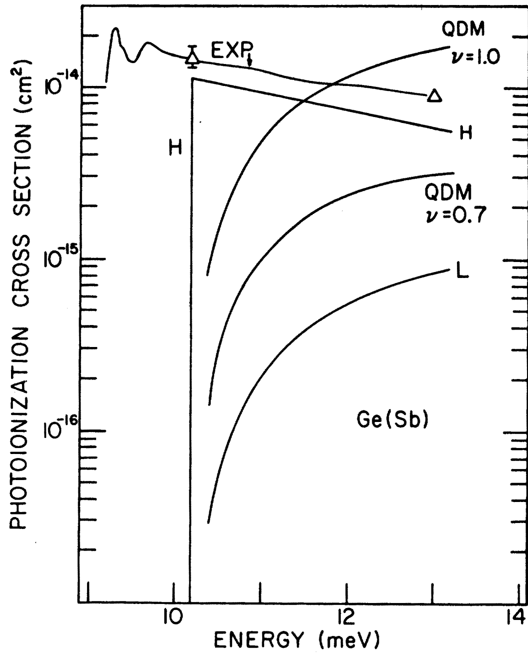

FIG. 14. Comparison of the photoionization-cross-section theories of the hydrogen model (H), Lucovsky model (L), and the quantum-defect method (QDM) with the experimental photoionization cross section (EXP) for Ge(Sb).

electrons, and the broad band over a limited range of the spectrum is not simply related to the number of conduction electrons. In order to determine the dependence of the occupation of a state on the pulsing current or pulsing field, careful analysis of more extensive measurements is required to resolve reliably the sharp emission bands at various currents.

C. Broad emission band

1. Electron capture cross section

It has been pointed out that the broad emission band at frequencies above the impurity ionization energy must be given by the recombination of conduction electrons with various impurity states. The spectral intensity of photon emission may be expressed by

$$I(\hbar\omega) = N^{+}\sum_{j}\sigma_{j}(\epsilon)v(\epsilon)f(\epsilon)\rho(\epsilon) \quad , \tag{4}$$

where $\epsilon = \hbar\omega - \epsilon_j$ is the energy of a conduction electron, ϵ_j is the ionization energy of the impurity state j, $\sigma_j(\epsilon)$ is the radiative capture cross section of the state j for the electron, $v(\epsilon)$ is the electron velocity, $\rho(\epsilon)$ is the density of states in the conduction band, and $f(\epsilon)$ is the distribution function of the conduction electrons. It will be shown that the contribution of the excited states is much smaller than that of the ground state. By neglecting the contribution of excited states it is possible to determine $f(\epsilon)$ from $I(\hbar\omega)$ if the cross section σ_0 of the ground state for the capture of conduction electrons is known. σ_0 is related to the cross section σ_0^ω for the capture of photons in the reverse process, i.e., opitcal excitation of electrons to the conduction band. The top curve in Fig. 14 gives σ_0^ω for Sb impurity deduced from the available absorption data; the ground-state splitting of Sb impurity is too small to be resolved. The cross section σ_0^ω for larger electron energies was obtained by a theoretical extension explained below.

It follows from the photoionization theory of hydrogen atoms[12] that for a hydrogenlike ground state with an ionization energy ϵ_0,

$$\sigma_0^\omega = \frac{1}{\eta}\frac{m}{m^*}\frac{2^7\pi h e^2}{3mc}\frac{1}{\epsilon_0}\left(\frac{\epsilon_0}{\epsilon_0+\epsilon}\right)^4 G(\epsilon) \;, \tag{5}$$

$$G(\epsilon) = \exp\left[-4(\epsilon_0/\epsilon)^{1/2}\arctan(\epsilon/\epsilon_0)^{1/2}\right] / \left[1 - e^{-2\pi(\epsilon_0/\epsilon)^{1/2}}\right], \tag{6}$$

Curve H in Fig. 14 is calculated according to this expression using $m^* = 0.19m$. A theory worked out by Lukovsky[13] using a δ-function core potential rather than the Coulomb potential of a hydrogenic model was found to fit the photoionization data of In in silicon but not the data of shallower impurities. Curve L is calculated according to this theory. The problem has been treated more recently[14] by a method using the quantum defect μ. This theory gives the wave function in terms of a parameter $\nu = (1-\mu)$ which fits the ionization energy ϵ_0 according to $\epsilon_0 = \epsilon_0^*/\nu^2$, where ϵ_0^* is the ionization energy in the effective-mass hydrogenic approximation. The cross section σ_0^ω was calculated using the Bloch function for the conduction band without the effect of the ionized impurity center. The two curves designated by QDM are calculated according to this theory for two values of the parameter ν. It is seen that even the curve for $\nu = 1$ is not the

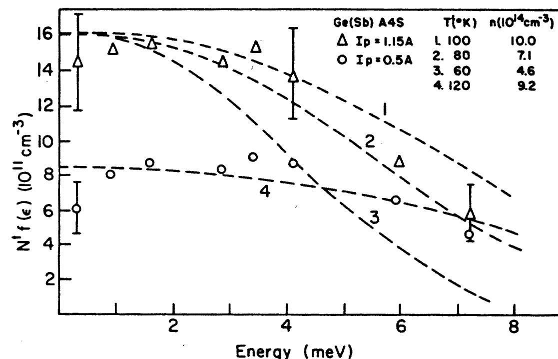

FIG. 15. Experimentally deduced $N^+f(\epsilon)$ are given by the points for two values of pulse current I_p. The curves are calculated according to Eq. (7) for various values of T_e' and n.

same as the curve H given by the hydrogenic approximation. In the energy range shown in Fig. 14, curve H is closest to the curve deduced from experimental data. Therefore, (5) was used to extend σ_0^ω to higher electron energies, with a coefficient of 1.15 which brings curve H to the top curve.

2. *Energy distribution of conduction electrons*

For Ge(Sb)-*A*4*S*, $N^+f(\epsilon)$ calculated from (4) and the measured $I(\hbar\omega)$ is shown by the points in Fig. 15 for two values of pulsing current I_p. Each set of points represents a curve different in shape from a Maxwell-Boltzmann distribution, more so for lower I_p. The departure shows that carrier-carrier scattering is not the sole dominant process in determining the energy distribution. Other processes are the interactions with phonons and the interactions, impact ionization, and Auger recombination involving the impurity. The interactions involving the impurity are usually considered to be unimportant for the distribution of carriers, for impurity concentrations around 10^{15} cm^{-1}.[15] The distribution determined by interaction with acoustic phonons has been considered by several authors. By considering only the emission of phonons, the distribution function obtained is[16]

$$f(\epsilon) = (n/2)(2\pi m^* kT_e'/h^2)^{-3/2}\, e^{-(\epsilon/kT_e')^{5/2}} \quad , \quad (7)$$

where

$$T_e' = T\left[\frac{\sqrt{2}}{6\pi}\left(\frac{16}{5}\frac{S}{\mu_a}\right)^2\left(\frac{m^*S}{kT}\right)^{1/2}\right]^{-2/5} E^{4/5} \quad , \quad (8)$$

E is the electric field, T is the lattice temperature, μ_a is the mobility at T as limited by acoustic phonons, and S is the velocity of sound. It has been shown that the distribution calculated with phonon absorption taken into account is close to that given by this expression, for $\epsilon < 8$ meV, which is the range of our interest. The dashed curves in Fig. 15 are $nf(\epsilon)$ calculated according to (7) for various sets of n and T_e'. Curve 4 fits reasonably well the points for $I_p = 0.5$ A. The value of T_e' is reasonable since it corresponds to $E = 10$–16 V/cm, as compared to the actual field of $E \sim 15$ V/cm at $I_p = 0.5$ A. The value of $n = 9.2\times10^{14}$ is also reasonable since it is close to the value $N_D/2 = 8\times10^{14}$, which is thought to be roughly the saturation of impact ionization.

Curves 1, 2, and 3 show that a curve for $T_e' \sim 90$ °K and an acceptable value of n would appear to fit the triangle points for $I_p = 1.15$ A. However, $T_e' \sim 90$ °K corresponds to $E \sim 7.5$ V/cm, whereas the field for $I_p = 1.15$ A was actually 22 V/cm. The hypothesis that the distribution is determined by acoustic phonon interaction is clearly not valid for $I_p = 1.15$ A. In general, the hypothesis gives a distribution more flattened at low energies as compared with a Maxwell-Boltzmann distribution. With increasing energy, the carrier-carrier scattering might be expected to increase its influence relative to the phonon interaction in determining the distribution. Consequently, the distribution may tend to approach a Maxwell-Boltzmann form. Such consideration is consistent with the fact that the points for ($I_p = 1.15$ A, $E = 22$ V/cm) in Fig. 15 seem to resemble a Maxwellian distribution more than the points for ($I_p = 0.5$ A, $E = 15$ V/cm).

Now we shall show that the contribution of excited states to the broad-band emission is indeed negligible. We have seen that the hydrogenic model gives a good approximation for σ_0^ω. The treatment of electron capture by a hydrogen atom has been extended to include excited states.[17] Using the expressions given by the treatment, we get the capture cross sections σ_j^ω for various excited states in the hydrogenic model, in a similar way as in the case of σ_0^ω. For the present purpose, the distribution function for $I_p = 1.15$ A may be approximated by a Maxwell-Boltzmann distribution, $e^{-\epsilon/kT}$, with $T \sim 80$ °K. The results calculated with these approximations are shown in Fig. 16. In the range beyond the beginning of the ground-state 1*s* contribution, the contributions of the excited states only amount to $\lesssim 10\%$ of the 1*s* contribution. The figure shows also that transitions of conduction

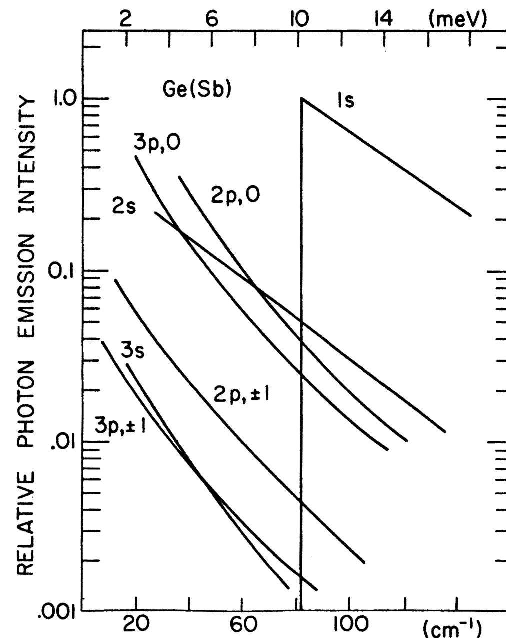

FIG. 16. Relative photon emission intensity for hot-electron transitions to various localized impurity levels for Ge(Sb). Wessel capture cross sections and Maxwell-Boltzmann statistics with $T_e = 81.5$ °K have been used as explained in the text.

electrons to the $2p, 0$ state with a threshold of $\sim 37\ cm^{-1}$, and to the $2s$ state with a threshold of $\sim 28\ cm^{-1}$, may show up in the observed spectrum. In fact, the shoulder at the low-frequency end of the spectra in Fig. 10 seems to be the combined effect of these transitions.

For the As-doped samples, emission exclusively due to conduction electrons begins at $\sim 113\ cm^{-1}$, which corresponds to transitions to the $1s(1)$ ground state. Such a region begins at $\sim 103\ cm^{-1}$ for P-doped germanium. Transitions of conduction electrons to the higher component $1s(3)$ of the split ground state may give broad emission above $\sim 79\ cm^{-1}$ in both cases. A broad background rising in this neighborhood is indeed indicated by the spectra in Figs. 11–13. Judging by the broad band due to conduction-electron $1s(1)$ transitions, a stronger indication of the transition to $1s(3)$ may be expected if $\sigma_{1s(1)}$ and $\sigma_{1s(3)}$ were both calculated according to the expression for a hydrogenic ground state. The discrepancy shows the inadequacy of the hydrogenic approximation for estimating σ's of a ground state with large splitting.

V. EMISSION SPECTRA OF GaAs

The emission spectra of GaAs-*E5S* are shown in Fig. 17. A beam splitter used in the path of emission had low transmission in the range corresponding to the dashed part of the spectra, reducing the reliability of the measurement. The large error bars represent the uncertainty due to low sensitivity of the GaAs detector in the high-energy range. The spectrum labeled M, taken from the publication of Melngailis *et al.*,[4] is included for comparison. The epitaxial GaAs studied by the previous authors had an impurity concentration 37 times smaller than that of our samples, and the electrical field used by them was below 8 V/cm, whereas the field used in our studies was in the range 10–44 V/cm. In the photoconductivity studies of Stillman *et al.*[18] on epitaxial GaAs with donor concentrations $\gtrsim 2\times10^{14}\ cm^{-3}$, peaks at 35.5, 42, and ~27 cm^{-1} were observed. The photoconductivity peaks at 35.5 and 42 cm^{-1} were attributed to $1s \to 2p$ and $1s \to 3p$ transitions, respectively, of a hydrogenic impurity. This interpretation was supported by an observed splitting of peaks in a magnetic field. With the assignment of the $2p$ level, the photoionization energy was estimated to be 47.3 cm^{-1} according to the effective-mass theory. Our spectra show all the features corresponding closely in energy to the peaks of photoexcitation and the onset of photoionization. It seems reasonable to adopt tentatively this interpretation for our results, keeping in mind that the nature of the impurity in our samples and the photoconductivity samples is not known. Only one pronounced peak is shown by the spectrum M, which apparently corresponds to the $2p \to 1s$ transitions. According to Melngailis *et al.*, the emission involving $3p$ and higher excited states broadened and merged with the continuum due to conduction electrons.

The peak at the low-energy end of our spectra seems to correspond to the unidentified peak of photoconductivity in the same region. The spectral response of our GaAs detector also shows a peak around the same wave number. The model underlying the above interpretation does not give a state at $\sim 27\ cm^{-1}$ above the ground state, and transitions between two excited states are unlikely to be detected in photoconductivity. The peak in question may be produced by a different impurity or impurity-defect complex in the epitaxial samples.

VI. POSSIBILITY OF STIMULATED EMISSION

Stimulated emission comes into consideration when the density of radiation in a frequency range corresponds to photon quantum number $n \gtrsim 1$ on the average for the radiation modes in that frequency range. The spectral intensity P_ν emitted by the sample, which can be deduced from the measured spectrum, is related to the average spectral intensity $\psi_\nu^{(s)}$ of energy density inside the sample

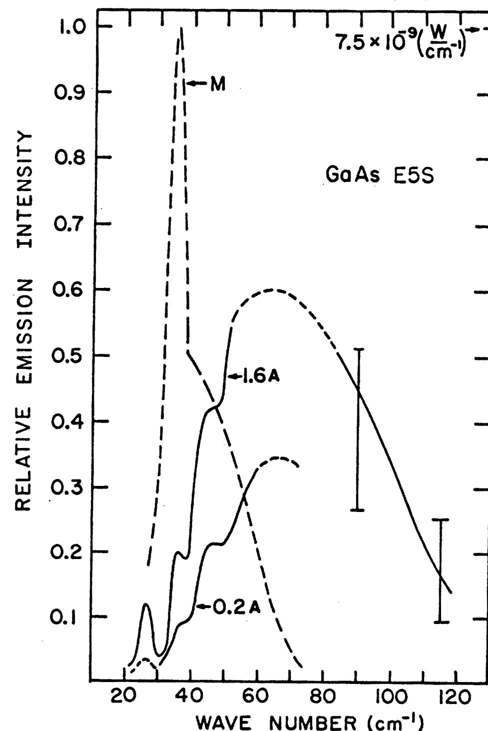

FIG. 17. Emission spectra for GaAs-*E5S* (1.6 and 0.2). The dashed curve M is taken from the measurements of Melngailis *et al.* (Ref. 4) for an epitaxial GaAs sample with an impurity concentration ~37 times less than that of the GaAs-*E5S* sample.

near the surface:

$$P_\nu = \tfrac{1}{4}c/\eta(1-R)A\psi_\nu^{(s)} \quad , \tag{9}$$

where η is the refractive index, A is the area of the emitting surface, and R is the surface reflectivity. With

$$\psi_\nu^{(s)} = 8\pi h\nu^3(\eta/c)^3 n_\nu^{(s)} \tag{10}$$

we get

$$P_\nu = (c\eta^2/4)(1-R)A8\pi h(\nu/c)^3 n_\nu^{(s)} \quad . \tag{11}$$

Examination of the spectra shows that the 63-cm^{-1} peak of Ge(Sb)-$A4S$ for $I_p = 1.15$ A corresponds to the highest n_ν encountered in the measurements. The measured power per unit wave number $P_k = cP_\nu = 2.8\times10^8$ W/cm^{-1} corresponds only to $n_\nu^{(s)} = 0.027$, which is too low for stimulated emission to be significant.

The generation G_ν of radiative power in the sample is balanced by the loss through emission, P_ν, from the sample and reabsorption A_ν in the sample:

$$A_\nu = c\alpha_\nu \int_V \psi_\nu dV = c\alpha_\nu \psi_\nu^{(V)} V \quad , \tag{12}$$

where α_ν is the absorption coefficient at frequency ν and $\psi_\nu^{(V)}$ is an average over the volume of the sample. Thus,

$$G_\nu = P_\nu + A_\nu = c[(\tfrac{1}{4}\eta)(1-R)A\psi_\nu^{(s)} + \alpha_\nu V\psi_\nu^{(V)}] \, . \tag{13}$$

The ratio of V/A is small for the samples measured, in particular $V/A = 0.02$ cm for Ge(Sb)-$A4S$. With $(\tfrac{1}{4}\eta)\,(1-R)\sim 0.64$ and a α_ν of the order of 1 cm^{-1}, reabsorption is negligible in comparison with emission from the sample in our measurements.

Under the rough approximation

$$\psi_\nu^{(s)} \sim \psi_\nu^{(V)} = \psi_\nu \quad , \tag{14}$$

we have

$$\psi_\nu = \frac{1}{c}\frac{G_\nu}{A}\,[\tfrac{1}{4}\eta(1-R) + \alpha_\nu(V/A)]^{-1} \quad .$$

According to this expression, $n_\nu \sim 1$ could be obtained at the 63-cm^{-1} peak of Ge(Sb), for example, with the generation rate of radiation achieved in our measurements if A is reduced by a factor of ~ 30. This condition requires making the sample into a cavity with low-loss, reflecting surfaces, except for a small emitting area.

†Supported in part by the U. S. Army Research Office—Durham, under Grant No. DA-ARO-D-31-124-72-G156.
*Present address: Dept. of Physics and Mathematics, Kentucky Wesleyan College, Owensboro, Ky. 42301.

[1]S. H. Koenig and R. D. Brown, III, Phys. Rev. Lett. 4, 170 (1960).
[2]G. Ascarelli and S. C. Brown, Phys. Rev. 120, 1615 (1960).
[3]S. N. Salomon and H. Y. Fan, Phys. Rev. B 1, 662 (1970).
[4]I. Melngailis, G. E. Stillman, J. O. Dimmock, and C. M. Wolfe, Phys. Rev. Lett. 23, 1111 (1969).
[5]E. Gornik, Phys. Rev. Lett. 29, 595 (1972).
[6]K. L. I. Kobayashi, K. F. Komatsubara, and E. Otsuka, Phys. Rev. Lett. 30, 702 (1973).
[7]A. M. Barnett, IBM J. Res. Dev. 13, 522 (1969).
[8]J. H. Reuszer and P. Fisher, Phys. Rev. 135, A1125 (1964).
[9]R. A. Faulkner, Phys. Rev. 184, 713 (1969).
[10]G. Ascarelli and S. Rodriguez, Phys. Rev. 124, 1321 (1961).
[11]F. Beleznay and G. Pataki, Phys. Status Solidi 13, 499 (1966).
[12]J. R. Oppenheimer, Phys. Rev. 31, 349 (1928).
[13]G. Lucovsky, Solid State Commun. 3, 299 (1965).
[14]H. B. Bebb, Phys. Rev. 185, 1116 (1969); H. B. Bebb and R. A. Chapman, J. Phys. Chem. Solids 28, 2087 (1967).
[15]J. Yamashita, J. Phys. Soc. Jap. 16, 720 (1961); A. Zylberstein, Phys. Rev. 127, 744 (1962); J. F. Palmier, Phys. Rev. B 6, 4557 (1972).
[16]R. Stratton, Proc. R. Soc. A 242, 355 (1957).
[17]W. Wessel, Ann. Phys. (N. Y.) 5, 611 (1930).
[18]G. E. Stillman, G. M. Wolfe, and J. O. Dimmock, *Proceedings of the Third International Conference on Photoconductivity, Stanford*, 1969 (Pergamon, New York, 1971), p. 265.